ELSEVIER

Thermochimica Acta 315 (1998) 169–179

thermochimica acta

Computer simulation of the Topley–Smith effect

Boris V. L'vov*, Alexander V. Novichikhin, Alexey O. Dyakov

Department of Analytical Chemistry, St. Petersburg State Technical University, St. Petersburg 195251, Russia

Received 3 September 1997; received in revised form 5 December 1997; accepted 2 February 1998

Abstract

Computer simulation of the layer-by-layer distribution of temperature and dehydration rate J in powdered $Li_2SO_4 \cdot H_2O$ monohydrate as functions of the partial pressure P_w of water vapor reveals a substantial self-cooling of the sample. The anomalous course of the $J=f(P_w)$ curve with increasing P_w, which manifests itself in the appearance of a maximum in the curve (the Topley–Smith effect), originates from the competition of the depressing action of H_2O vapor on the dehydration rate with increasing heat transfer from the furnace to the sample. The model accounts for the main features of the Topley–Smith effect, namely, the falloff of decomposition rate for low P_w and the minimum in the $J=f(P_w)$ curve, the variation of the value of P_w corresponding to the maximum of the curve within two orders of magnitude for different hydrates, and the enhancement of the effect with increasing decomposition temperature and decreasing grain size of the powder sample. © 1998 Elsevier Science B.V.

Keywords: Computer simulation; Dehydration of $Li_2SO_4 \cdot H_2O$; Self-cooling effect; Topley–Smith effect

1. Introduction

Anomalous variation of the rate of dehydration (J) of crystalline hydrates with increasing water-vapor pressure (P_w) was discovered by Topley and Smith (T–S) in 1931 [1] in a study of the rate of dehydration of $MnC_2O_4 \cdot 2H_2O$. An excellent description of the essence and possible mechanisms of this effect can be found in Ref. [2]. In the time elapsed thereafter, the T–S effect was observed in a score of different crystalline hydrates [3–17] (see Table 1). The most sizable contribution to its investigation is due to Frost et al. [5–8] in the 1950 s and to Bertrand et al. [11–13] in the 1970 s. Nevertheless, there is still no universally accepted explanation of the nature of this phenomenon which would account for the shape of the $J=f(P_w)$ curve and for the specific features of its manifestation under variation of the measurement conditions, namely, dehydration temperature, sample mass, powder grain size, the presence in the reactor of foreign gases, etc. Out of the four or five different mechanisms proposed by various researchers, one most frequently invokes recrystallization of the product in the presence of H_2O put forward by Volmer and Seydel [4]. This mechanism assumes, in the course of recrystallization, the formation of additional channels, cracks and pores between the product particles, which favor evolution of water vapor from the reaction region and, as a consequence, an increase of the decomposition rate.

The model proposed by Bertrand et al. [3], which is based on assuming a spatial thermal gradient in the

*Corresponding author. Tel.: 007 812 5527741; fax: 007 812 5280281; e-mail: lvov@achem.hop.stu.neva.ru

PII S0040-6031(98)00296-2

Table 1
The Topley–Smith effect studies

Reactant	Product	T/°C	Diameter of grains/ μm	P_w/Torr		Ref. and year of publication
				min	max	
$MnC_2O_4{\cdot}2H_2O$	MnC_2O_4	76		0.1	1.0	[1] (1931)
$MnC_2O_4{\cdot}2H_2O$	MnC_2O_4	76	88	0.125	0.96	[3] (1935)
$MnC_2O_4{\cdot}2H_2O$	MnC_2O_4	60		0.061	0.26	[4] (1937)
$ZnSO_4{\cdot}6H_2O$	$ZnSO_4{\cdot}H_2O$	45	310–420	0.8	1.55	[5] (1951)
$CuSO_4{\cdot}5H_2O$	$CuSO_4{\cdot}H_2O$	40	310–420	0.3	3.4	[6] (1953)
$MnSO_4{\cdot}4H_2O$	$MnSO_4{\cdot}H_2O$	40	310–420	1.1	3.0	[7] (1955)
$ZnSO_4{\cdot}7H_2O$	$ZnSO_4{\cdot}H_2O$	40	310–420	1.5 [a]	4.0 [a]	[7] (1955)
$FeSO_4{\cdot}7H_2O$	$FeSO_4{\cdot}H_2O$	60	310–420	6	8	[7] (1955)
$Ni(NO_3)_2{\cdot}7H_2O$	$Ni(NO_3)_2{\cdot}2H_2O$	50	310–420	2.5	2.9	[7] (1955)
$MgSO_4{\cdot}7H_2O$	$MgSO_4{\cdot}H_2O$	40	310–420	5	7	[7] (1955)
$NiSO_4{\cdot}6H_2O$	$NiSO_4{\cdot}H_2O$	—[b]	310–420	—[b]	—[b]	[7] (1955)
$MgSO_4{\cdot}7H_2O$	$MgSO_4{\cdot}H_2O$	40	310–420	4	15	[8] (1956)
$CoCl_2{\cdot}6H_2O$	$CoCl_2{\cdot}H_2O$	30	310–420	—	0.7	[8] (1956)
$CaSO_4{\cdot}0.5H_2O$	$CaSO_4$	140	64–75	5	17	[9] (1970)
$CaC_2O_4{\cdot}H_2O$	CaC_2O_4	120	120–150	0.5	1	[10] (1970)
$CuSO_4{\cdot}5H_2O$	$CuSO_4{\cdot}H_2O$	31		0.4	1.3	[11] (1972)
$Li_2SO_4{\cdot}H_2O$	Li_2SO_4	86	90–100	1.7	2	[12] (1974)
$MgSO_4{\cdot}4H_2O$	$MgSO_4{\cdot}2H_2O$	86	<63	8	30	[12] (1974)
$CuSO_4{\cdot}5H_2O$	$CuSO_4{\cdot}3H_2O$	52	63–90	1	6	[12] (1974)
$CuSO_4{\cdot}3H_2O$	$CuSO_4{\cdot}H_2O$	54	<40	0.2	3	[12] (1974)
$NaB_4O_5(OH)_4{\cdot}8H_2O$	$NaB_4O_5(OH)_4$	38	63–90	5	12	[12] (1974)
$CuSO_4{\cdot}5H_2O$	$CuSO_4{\cdot}3H_2O$	45	15–20	1	3	[13] (1978)
$MgC_2O_4{\cdot}2H_2O$	MgC_2O_4	114	120–150	0.5	2	[14] (1978)
$Zn(HCO_2)_2{\cdot}2H_2O$	$Zn(HCO_2)_2$	100	160–250	—	0.7	[15] (1989)
$Er(HCO_2)_2{\cdot}2H_2O$	$Er(HCO_2)_2$	124	250–310	—	0.5	[16] (1992)
$BaCl_2{\cdot}2H_2O$	$BaCl_2{\cdot}H_2O$	44	53–63	0.7 [c]	1.2 [c]	[17] (1995)

[a] Two minima and two maxima were observed: at 0.2 and 0.7, and 1.5 and 4.0 Torr.
[b] Similar to $MgSO_4{\cdot}7H_2O$ [7].
[c] Our estimation based on the original data of Ref. [17].

reaction zone, did not receive as much recognition. In this model, the anomalous increase of the rate of decomposition with P_w is ascribed to the increasing rate of heat transfer from the heater to the reactant, whose temperature is lower as a result of the self-cooling effect. The mechanism was convincingly supported by model calculations and experiments with an evaporator–condenser system using ethanol and water for illustration. In these experiments, the temperature of the evaporating liquid was found to be much lower than that of the evaporator. In case of ethanol, e.g. the difference from the thermostat temperature (300 K) was as high as 45 K or 15%. For reasons which remain unclear, this model did not enjoy further development in the subsequent 20 years of investigation of the T–S effect. One may only conjecture that the existence of an enormous difference in temperature between a crystalline hydrate sample and the heater was considered by many researchers to be just impossible.

Presently, the situation has changed. It was shown [18] that the heating of powder samples being decomposed in vacuum is extremely nonuniform, so that the ratio of the temperatures of the heater and the innermost layer in the powder sample may be as high as 1.5 or even more. The nonuniformity of heating increases with the number of layers n of the powder sample and decomposition temperature. For instance, in the case of $Mg(OH)_2$, decomposing at a heater temperature of 600 K, the calculated temperature of the innermost

powder layer is 480 K for n=100 layers and 387 K for n=10^4, whereas for the heater temperature of 500 K the corresponding values are, respectively, 473 K and the same 387 K.

In view of the above, as well as taking into account the scheme developed in Ref. [18] for calculating the rate of decomposition of a nonuniformly heated powder sample in vacuum, we have attempted to carry out a theoretical calculation of the J=$f(P_w)$ relation using for illustration the dehydration mechanism proposed [19] for $Li_2SO_4{\cdot}H_2O$.

2. Theoretical

2.1. Pressure dependence of heat flux

The heat expended in decomposing a powder sample in a stationary regime is compensated by the radiation emitted by the heater and powder grains and through heat transfer by the gas molecules. According to the Stefan–Boltzmann law, radiative heat transfer depends only on the temperature of the surfaces involved and does not depend on the gas pressure in the reactor. At low pressures, the heat flux J_q transported by gas molecules is proportional to the number of molecular collisions with the surface and the temperature difference ΔT between the adjacent powder layers:

$$J_q = \frac{\gamma P C_v \Delta T}{(2\pi MRT)^{1/2}} \tag{1}$$

where C_v is the molar heat capacity at constant volume, γ the coefficient of conversion from atmospheres to pascals, M the molar mass of the gas and R the gas constant.

The heat flux continues to grow with pressure until the mean free path λ becomes equal to the separation between the powder grain layers [20]. Further growth of P no more affects J_q. The quantity λ can be derived from the equation

$$\lambda = \frac{1}{4\sqrt{2}\pi r^2 N} \tag{2}$$

where r and N are the radius of molecules and their number in 1 m^3, respectively, [20].

The magnitude of r is about the same for the H_2O and N_2 molecules, namely 1.75×10^{-10} m [20]. Expressing N through pressure (in atm) and gas temperature and inserting the value of r in Eq. (2), we arrive at

$$\lambda = 2.5\times10^{-10} T/P \tag{3}$$

For instance, for T=400 K and P=10^{-2} atm, λ=1×10^{-5} m=10 μm.

2.2. Modeling of temperature distribution

In simulating the temperature distribution inside a powder sample, we used the same approach as before [18]. The sample was considered as consisting of horizontal layers of material of thickness equal to the powder grain diameter. Thus, simulation of the temperature distribution inside a powder sample can be reduced to modeling the vertical temperature distribution between layers of this substance. If the furnace temperature is the same on top and at the bottom of the sample, the analysis can be limited to considering only one half of such a multilayered sample, from the central, 0th or 1st layer, to the outermost nth layer.

Disregarding heat conduction through point contacts among the grains and assuming a steady-state decomposition, we can write for an ith layer the following equality between the amount of heat expended for the decomposition, radiation and heat transfer through water vapor and residual air and that received in the form of radiation and heat transfer from the adjacent ($i-1$)th and ($i+1$)th layers:

$$\begin{aligned} 2AT_i^{-1/2}&\left[\left(\frac{P_w^2}{4}+B\exp\frac{E}{T_i}\right)^{1/2}-\frac{P_W}{2}\right] \\ &+2CT_i^4+D_wT_i^{-1/2}P_w(T_i-T_{i-1}) \\ &+D_aT_i^{-1/2}P_a(T_i-T_{i-1}) \\ &=C(T_{i-1}^4+T_{i+1}^4)+D_wT_i^{-1/2}P_w(T_{i+1}-T_i) \\ &+D_aT_i^{-1/2}P_a(T_{i+1}-T_i) \end{aligned} \tag{4}$$

where

$$A \equiv \frac{\gamma\Delta H_T^0}{(2\pi M_p R)^{1/2}} \tag{5}$$

$$B \equiv \exp\frac{\Delta S_T^0}{R} \tag{6}$$

$$C \equiv \varepsilon\sigma \tag{7}$$

$$D_w \equiv \frac{\gamma C_{vw}}{(2\pi M_w R)^{1/2}} \tag{8}$$

$$D_a \equiv \frac{\gamma C_{va}}{(2\pi M_a R)^{1/2}} \tag{9}$$

and

$$E \equiv -\frac{\Delta H_T^0}{R} \tag{10}$$

Here ΔH_T^0 and ΔS_T^0 are, respectively, the changes of the enthalpy and entropy in the decomposition process, P_w and P_a the external pressure of the water and air, M_p, M_w, M_a the molar masses of the product, water and air, C_{vs} and C_{va} the molar heat capacities of water and air, ε the emittance of the grain surface and σ the Stefan–Boltzmann constant. The expression in square brackets corresponds to the partial pressure of the product for comparable values of external and internal partial pressures of water [18].

Eq. (4) can be conveniently recast in the form

$$C(T_{i+1}^4 - 2T_i^4 + T_{i-1}^4) + (D_w P_w + D_a P_a) \times T_i^{-1/2}(T_{i+1} - 2T_i + T_{i-1}) = 2AT_i^{-1/2}\left[\left(\frac{P_w^2}{4} + B\exp\frac{E}{T_i}\right)^{1/2} - \frac{P_w}{2}\right] \tag{11}$$

For the central (i=0 or i=1), the coldest layer, one should write the following additional boundary condition

$$T_{i+1} = T_{i-1} \tag{12}$$

if the total number of layers is odd (n_t=2n+1), or

$$T_i = T_{i-1} \tag{13}$$

if it is even (n_t=2n). Thus, Eq. (11) takes on the form

$$C(T_1^4 - T_0^4) + (D_w P_w + D_a P_a)T_1^{-1/2}(T_1 - T_0) = AT_0^{-1/2}\left[\left(\frac{P_w^2}{4} + B\exp\frac{E}{T_i}\right)^{1/2} - \frac{P_w}{2}\right] \tag{14}$$

for the case (12), and

$$C(T_2^4 - T_1^4) + (D_w P_w + D_a P_a)T_1^{-1/2}(T_2 - T_1) = 2AT_1^{-1/2}\left[\left(\frac{P_w^2}{4} + B\exp\frac{E}{T_i}\right)^{1/2} - \frac{P_w}{2}\right] \tag{15}$$

for the case (13). Eqs. (14) and (15) permit one to determine the temperature of the layer adjacent to the coldest layer, if the temperature of the latter is prescribed arbitrarily (T_0 or T_1). The temperatures of all the other layers can be sequentially calculated from Eq. (11), with due account of the fact that the temperature of the (n+1)st layer should coincide with that of the furnace. To do this, one should vary T_0 or T_1 appropriately while keeping the other conditions constant.

2.3. Simulation of $J=f(P_w)$ curve

The calculations were completed by constructing $J=f(P_w)$ curves, which relate the rate of dehydration of $Li_2SO_4{\cdot}H_2O$ to the external partial pressure of water with the other variable parameters, namely, furnace temperature, partial pressure of residual gas (air) and the number of layers in the powder sample.

The resultant decomposition rate was calculated using the Hertz–Knudsen–Langmuir equation while taking into account the layer-by-layer distribution of temperature T_i:

$$J = \frac{\gamma M_r \sum_{i=1}^{n} T_i^{-1/2}[(P_w^2/4 + B\exp(E/T_i))^{1/2} - P_w/2]}{(2\pi M_p R)^{1/2}} \tag{16}$$

where M_r is the molar mass of the reactant and the bracketed expression corresponds, as before, to the partial pressure of the product for comparable values of the external and internal partial pressures of water [18].

The decrease in the rate of decomposition under nonuniform heating of the powder (J_n) relative to the rate found under uniform heating of the powder (J_u) up to the furnace temperature was calculated using the obvious relationship

$$\frac{J_n}{J_u} = \frac{\sum_{i=1}^{n} T_i^{-1/2}[(P_w^2/4 + B\exp(E/T_i))^{1/2} - P_w/2]}{nT_f^{-1/2}[(P_w^2/4 + B\exp(E/T_f))^{1/2} - P_w/2]} \tag{17}$$

2.4. Selection of initial parameters

Table 2 lists all the data required to calculate the temperature and rate of the following reaction

$$Li_2SO_4 \cdot H_2O(s) \rightarrow Li_2SO_4(g) + H_2O \tag{18}$$

Table 2
Parameters used in the calculations

Parameter	Symbol	Value
Molar mass of $Li_2SO_4 \cdot H_2O$	M_r	0.124 kg mol^{-1}
Molar mass of Li_2SO_4	M_p	0.106 kg mol^{-1}
Molar mass of H_2O	M_w	0.018 kg mol^{-1}
Molar mass of air (N_2)	M_a	0.028 kg mol^{-1}
Enthalpy of reaction (18)	ΔH^0_{298}	193.8 kJ mol^{-1}
Entropy of reaction (18)	ΔS^0_{298}	350.5 J mol^{-1} K^{-1}
Molar heat capacity of air	C_{va}	20.8 J mol^{-1} K^{-1}
Molar heat capacity of H_2O vapor	C_{vw}	27.4 J mol^{-1} K^{-1}
Gas constant	R	8.3145 J mol^{-1} K^{-1}
Stefan–Boltzmann constant	σ	5.6705×10^{-8} W m^{-2} K^{-4}
Emittance	ε	0.62
Pressure conversion factor	γ	101325 Pa atm^{-1}

The enthalpy of reaction (18) is given while taking into account the partial transfer of the energy released in Li_2SO_4(g) condensation to the reactant at $\tau=0.6$ [19]. By analogy with MgO [18], the value of ε was taken equal to 0.62. The values of C_{vw} and C_{va} were chosen in accordance with the experimental data presented in Ref. [20].

2.5. Computer program

The program is written in Visual Basic for Windows. The flow chart of the calculation algorithm is shown in Fig. 1. After putting in the calculation parameters, namely, the furnace temperature T_f, total number of layers n, water-vapor pressure P_w, foreign-gas pressure P_a, the parameters derived from fundamental constants, A, B, C, D and E and the temperature of the first layer, which in the initial stage was taken equal to $T_f/2$, the temperature of the second layer was calculated by the iterative procedure, using Eq. (15). The variable parameter was T_2, the first approximation being $T_2=T_1$. The iterations are continued until the difference between the left, L, and the right, R, parts of Eq. (15) in absolute value become $<10^{-9}$. Next, the temperatures of all subsequent layers, T_3 to T_{n+1}, were calculated in a similar way, using Eq. (11). The initial temperature of each subsequent layer T_{i+1} was taken equal to that of the preceding layer, T_i. After terminating the calculations, the temperature of the $(n+1)$th layer was compared with that of the furnace. If the condition $|T_f-T_{n+1}|\leq 0.01$ was met, the calculation was considered completed, otherwise the temperature of the first layer was either reduced (for $T_f<T_{n+1}$) or increased (for $T_f>T_{n+1}$), and the calculations resumed. The temperature T_1 was varied in steps of 10^m, with m reduced by unity on each reversal of the T_f-T_{n+1} difference in sign. The first approximation was $m=2$. If calculations were performed for different water-vapor pressures ($P_{start} \neq P_{end}$), the above procedure was repeated for each new value of P_w, which was varied from $P_{start}=10^{-5}$ atm to $P_{end}=10^{-2}$ atm with an exponent step of 0.02. The results were displayed on the monitor in the form of graphs and tables with their subsequent recording on the disk.

3. Results and discussion

The above program and the parameters listed in Table 2 were used to perform extensive calculations of the temperature and rate of dehydration of $Li_2SO_4 \cdot H_2O$ as functions of the number of layers of a powder sample, furnace temperature, and partial pressures of water vapor and residual air. The main results of these calculations are presented below in the form of graphs and tables.

Although the presence of water vapor or air significantly reduces the self-cooling compared to the vacuum conditions, it does not provide isothermal conditions for decomposition. This is clearly seen from Figs. 2 and 3, which show the layer-by-layer temperature distribution in powder sample against P_w

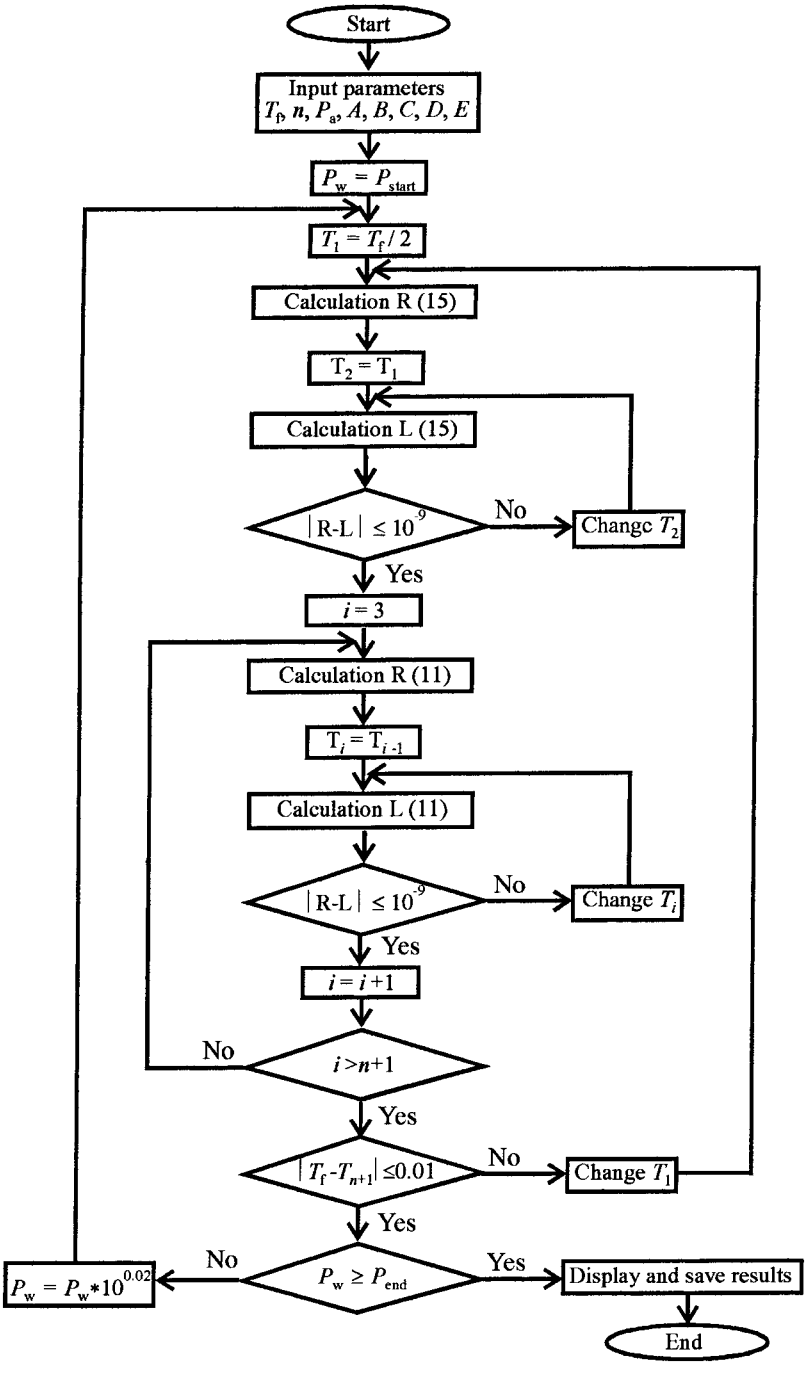

Fig. 1. Flow chart of the calculation program.

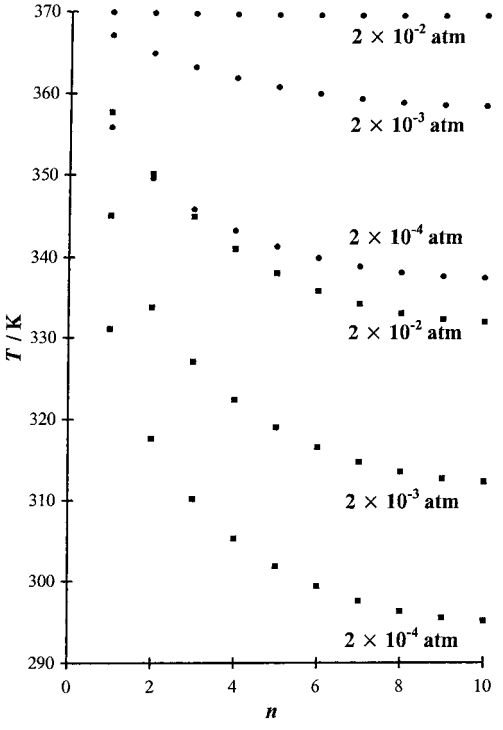

Fig. 2. Calculated temperature distribution for a $Li_2SO_4{\cdot}4H_2O$ powder at T_f=370 K and n=10 for the different values of (●) P_w and (■) P_a.

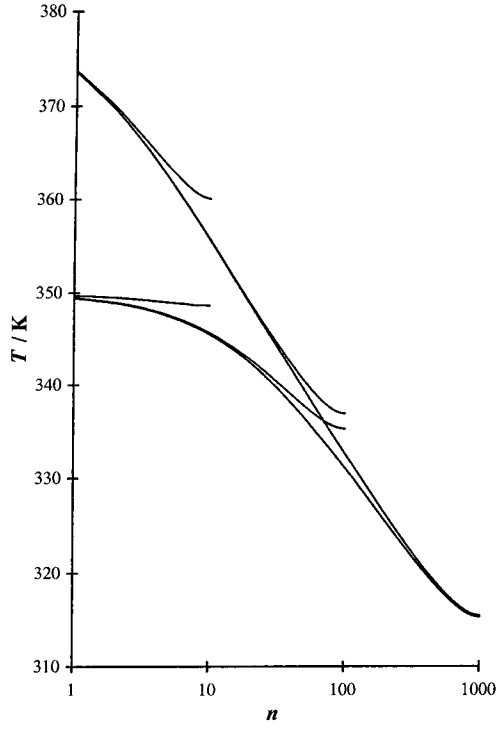

Fig. 3. Calculated temperature distribution for a $Li_2SO_4{\cdot}H_2O$ powder at 350 and 380 K furnace temperatures and $P_w=2\times10^{-3}$ atm for different number of layers: 10, 100 and 1000.

and P_a for n=10 (Fig. 2) and as functions of n and T_f for $P_w=2\times10^{-3}$ (Fig. 3). The nonuniformity of powder heating grows with n and T_f. In the presence of air, the temperature nonuniformity turns out to be much larger than that in water vapor (Fig. 2), since H_2O reduces the rate of decomposition of the hydrate and, hence, the sample self-cooling.

To illustrate the effect of self-cooling on the rate of decomposition, Table 3 lists the calculated decrease of the rate of dehydration of $Li_2SO_4{\cdot}H_2O$ relative to the rate under isothermal conditions for different n and T_f. The value of P_w was chosen as 0.002 atm, which approximately corresponds to the maximum in the experimental $J=f(P_w)$ curve for $Li_2SO_4{\cdot}H_2O$ [9]. We see, however, that even in this case the reduction in rate of decomposition is quite noticeable, particularly for large n and T_f.

Consider now the shape of the $J=f(P_w)$ curves, a problem of primary importance in our study. In full agreement with experimental observations, the increase of P_w from 10^{-5} to 10^{-2} atm results, contrary to the monotonic decrease of rate of dehydration expected to occur in these conditions [19], in its growth and the appearance of a maximum in the $J=f(P_w)$ curves. This is due to an increase of heat transfer by H_2O vapor and a decrease of the self-cooling effect. The T–S effect becomes more pronounced as T_f and n become larger (see Figs. 4 and 5),

Table 3
Reduction in rate of decomposition of $Li_2SO_4{\cdot}H_2O$ as a result of self-cooling effect at P_w=0.002 atm (calculated in accordance with Eq. (17))

n	J_n/J_u			
	350 K	360 K	370 K	380 K
1	0.996	0.982	0.911	0.700
10	0.827	0.521	0.245	0.098
100	0.167	0.066	0.026	0.010

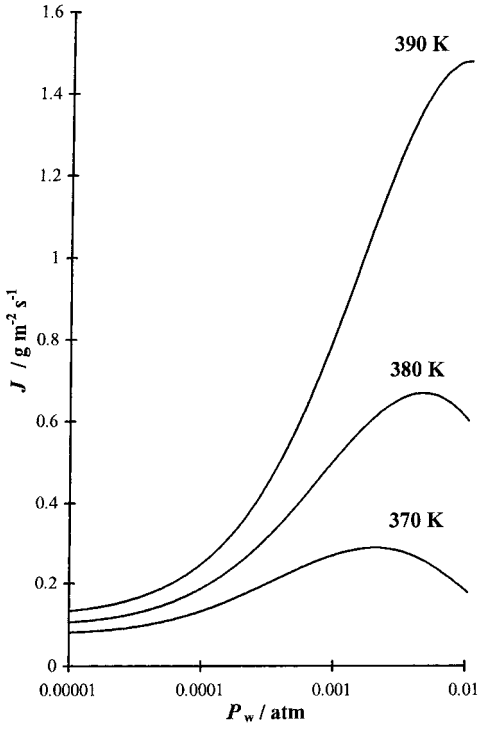

Fig. 4. Rate of decomposition of a $Li_2SO_4{\cdot}H_2O$ powder (n=10) as a function of partial pressure of water at different furnace temperatures.

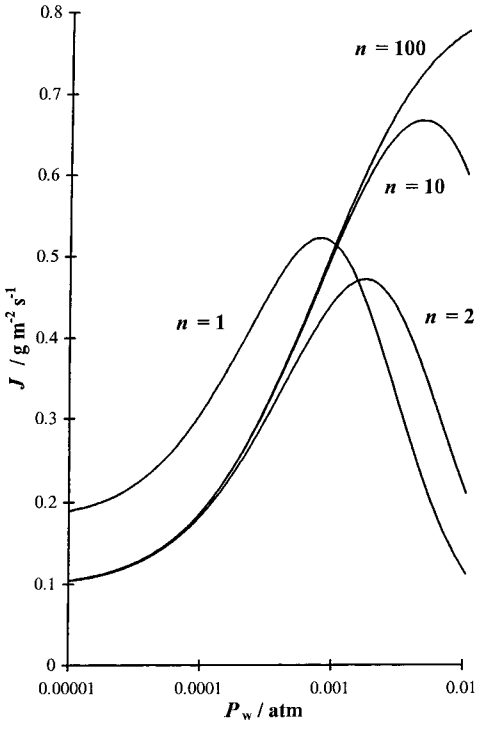

Fig. 5. Rates of decomposition of a $Li_2SO_4{\cdot}H_2O$ single crystal (n=1) and powders (n=2, 10 and 100) as functions of partial pressure of water at T_f=380 K.

which is likewise in agreement with experiment [12,13], in particular, with the enhancement of the T–S effect with decreasing grain size [13]. Nevertheless, a comparison of the calculated $J=f(P_w)$ curves in Figs. 4 and 5 with experimental relations found for $Li_2SO_4{\cdot}H_2O$ [12] reveals substantial differences in their shapes. First, the initial part of the experimental curves exhibits a decrease in the rate of dehydration with increasing P_w and the formation of a minimum. Second, the falloff of the dehydration rate after the maximum occurs much faster than it does in the calculated relations, so that the maximum in the experimental $J=f(P_w)$ curves turns out to be sharper.

The reason for the first of the two above-mentioned differences lies most probably in the presence of residual air in the reaction system, which takes part in heat transfer and reduces the self-cooling effect. In this case, addition of H_2O vapor for $P_w<P_a$ should result only in a decrease of the rate of dehydration. This is supported by the curves in Fig. 6, which were calculated for the same temperature of 380 K as those in Fig. 5, but with inclusion of air present at pressures of 10^{-4}, 3×10^{-4} and 10^{-3} atm. At the same time, it should be pointed out that there is no such initial decrease in the rate of dehydration for $CoCl_2{\cdot}6H_2O$ [8], $Zn(HCO_2)_2{\cdot}2H_2O$ [15] and $Er(HCO_2)_2{\cdot}2H_2O$ [16], so that the experimental $J=f(P_w)$ curves resemble, in this case, more the calculated curves in Figs. 4 and 5 than those in Fig. 6.

The most probable reason for the second of the above-mentioned discrepancies lies in that an increase in P_w acts on heat transport only to a certain extent, where the mean free path of molecules (λ_{max}) at the maximum of the $J=f(P_w)$ curve becomes equal to the distance between the powder grain layers. This distance can be taken as about equal to half the grain diameter, $d/2$, whence

$$\lambda_{max} \cong d/2 \tag{19}$$

Fig. 7 displays $J=f(P_w)$ graphs plotted on logarithmic

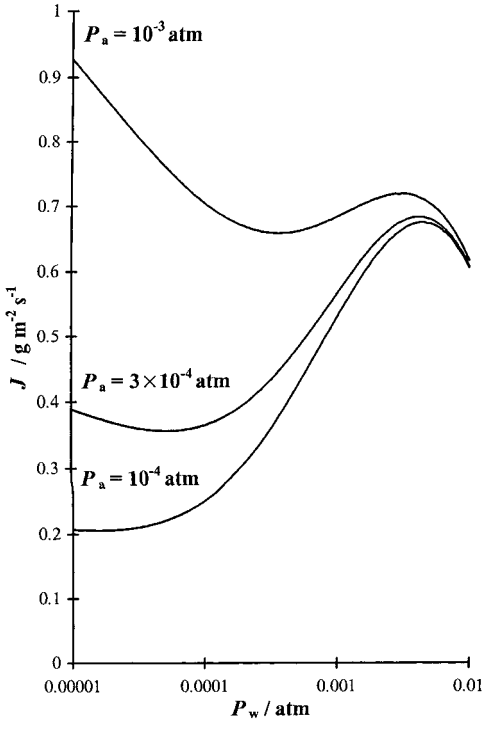

Fig. 6. Rate of decomposition of $Li_2SO_4{\cdot}H_2O$ powder (n=10) as a function of partial pressure of water at T_f=380 K for different partial pressures of air.

and linear scales, which were calculated for $P_a=10^{-3}$ atm and take into account the increase of heat transfer by water vapor up to $P_w=2\times10^{-3}$ atm (1.52 Torr). Above 2×10^{-3} atm, heat transfer is assumed to be constant. When this is taken into account, the falloff after the maximum becomes sharper, and the maximum, more pronounced. (In real conditions, the boundary corresponding to maximum heat transfer can be fairly diffuse because of the polydisperse nature of the powder and the dependence of this critical value of P_w on temperature. This can be seen from relation (3).)

The foregoing mechanism, responsible for the maximum, permits one to explain the fairly broad variation in the values of $(P_w)_{max}$, which correspond to the maxima in the $J=f(P_w)$ curves, observed for different crystalline hydrates and, in some cases, also the differences between the values of $(P_w)_{max}$ found for the same crystalline hydrate (see Table 1). To the extreme values of $(P_w)_{max}$, which are 0.26 Torr for $MnC_2O_4{\cdot}2H_2O$ [4] and 30 Torr for $MgSO_4{\cdot}4H_2O$ [12], correspond, according to Eq. (3), the values of λ_{max} and, hence, of grain radius $d/2$, respectively, equal to 240 and 2.3 μm. In many cases, the values of λ_{max}, calculated using Eq. (3), agree fairly satisfactorily (within a factor of two) with the average grain radii quoted in the corresponding publications {for $MnC_2O_4{\cdot}2H_2O$ see Ref. [3], for $CoCl_2{\cdot}6H_2O$ see Ref. [8], for $CaC_2O_4{\cdot}H_2O$ see Ref. [10], for $LiSO_4{\cdot}H_2O$ see Ref. [12], for $CuSO_4{\cdot}3H_2O$ see Ref. [12], for $CuSO_4{\cdot}5H_2O$ see Ref. [13], for $MgC_2O_4{\cdot}2H_2O$ see Ref. [14], for $Zn(HCO_2)_2{\cdot}2H_2O$ see Ref. [15], for $Er(HCO_2)_2{\cdot}2H_2O$ see Ref. [16] and for $BaCl_2{\cdot}2H_2O$ see Ref. [17]}. At the same time, the calculations were found to disagree strongly with experiment in some cases. For $ZnSO_4{\cdot}6H_2O$ [5], $CuSO_4{\cdot}5H_2O$ [6], $MnSO_4{\cdot}4H_2O$ [7], $ZnSO_4{\cdot}7H_2O$ [7], $FeSO_4{\cdot}7H_2O$ [7], $Ni(NO_3)_2{\cdot}7H_2O$ [7], $MgSO_4{\cdot}7H_2O$ [7,8], $MgSO_4{\cdot}4H_2O$ [12] and $NaB_4O_5(OH)_4{\cdot}8H_2O$ [12], the calculated values of λ_{max} were found to lie below the grain radius by an order of magnitude. This is possibly due to the fact that the sizes quoted in the papers related to the starting, nondecomposed powder grains. As a result of formation of smaller particles in the course of decomposition (a few tenths of a μm in size [21]), the distance between grains in the reactant-product mixture decreases.

4. Conclusions

Calculations of the self-cooling effect have shown that, even in the presence of foreign gases, self-cooling can bring about a substantial reduction in the rate of decomposition compared to its value expected for isothermal conditions. For powders, this effect should be more pronounced than for single crystals. These conclusions should be taken into account in choosing experimental conditions of kinetic measurements and interpreting the results obtained.

Simulation of the dependence of the rate of dehydration J on water-vapor pressure has shown that the anomalous behavior of the $J=f(P_w)$ relation with increasing P_w, which consists in the appearance of a maximum in the curve, is actually the result of competition between the depressing influence of water vapor on dehydration, on the one hand, and the increasing heat transfer from the furnace to the sample by water vapor, on the other, in the presence of intense self-cooling. The value of P_w, corresponding to the maxi-

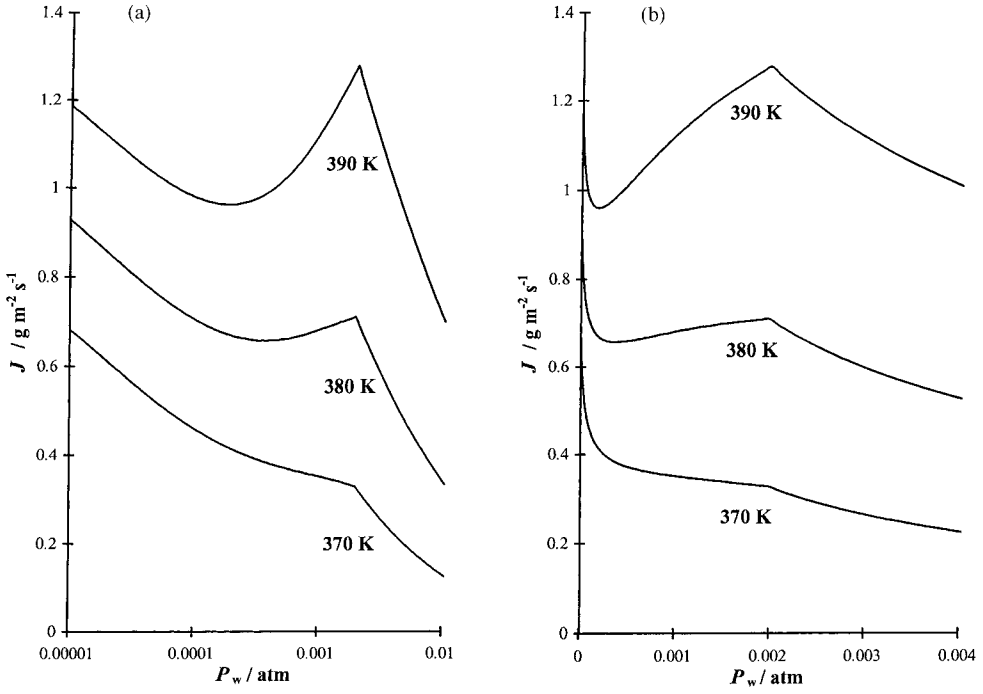

Fig. 7. Rate of decomposition of $Li_2SO_4{\cdot}H_2O$ powder (n=10) as a function of partial pressure of water at $P_a=10^{-3}$ atm and $(P_w)_{max}=2\times10^{-3}$ atm in the (a) logarithmic and (b) linear P_w scales.

mum in J in the curve, is determined by the powder grain size. The initial fall in the $J=f(P_w)$ curve observed at small P_w is most probably due to the presence of residual air in the reaction system, which reduces the contribution of water vapor to heat transfer for $P_w<P_a$. The calculations offer an explanation for other experimentally observed features of the T–S effect as well, in particular, for the enhancement of the effect with increasing decomposition temperature and decreasing powder grain size.

Among the problems, that still await solution, is how the T–S effect influences the coefficient τ [19]. To find an answer, one should first explain the mechanism of the partial transfer of the energy released in condensation of a non-volatile product. Simulation of the T–S effect for crystalline hydrates containing several water molecules would undoubtedly be of considerable interest. Among experimental studies, essential for further development of the theory, is the investigation of the dependence of the maximum in the $J=f(P_w)$ relation on experimental conditions, as well as observation of this effect in other compounds, for instance hydroxides.

Acknowledgements

The authors thank Professor A.K. Galwey for his interest and stimulating comments to this paper. This work was supported by BSW Perkin–Elmer.

References

[1] B. Topley, M.L. Smith, Nature 128 (1931) 302.
[2] M.E. Brown, D. Dollimore, A.K. Galwey, Reactions in the Solid State, Elsevier, Amsterdam, 1980.
[3] B. Topley, M.L. Smith, J. Chem. Soc. (1935) 321.
[4] M. Volmer, G. Seydel, Z. Phys. Chem. A 179 (1937) 153.
[5] G.B. Frost, K.A. Moon, E.H. Tompkins, Can. J. Chem. 29 (1951) 605.
[6] G.B. Frost, R.A. Campbell, Can. J. Chem. 31 (1953) 107.
[7] R.C. Weeler, G.B. Frost, Can. J. Chem. 33 (1955) 546.
[8] R.W. Ford, G.B. Frost, Can. J. Chem. 34 (1956) 591.
[9] M.C. Ball, R.G. Urie, J. Chem. Soc. A (1970) 528.
[10] D. Dollimore, T.E. Jones, P. Spooner, J. Chem. Soc. A (1970) 2809.
[11] M. Lallemant, G. Bertrand, G. Watelle-Marion, C.R. Acad. Sci., Paris, C 275 (1972) 519.

[12] G. Bertrand, M. Lallemant, G. Watelle-Marion, J. Inorg. Nucl. Chem. 36 (1974) 1303.
[13] G. Bertrand, M. Lallemant, A. Mokhlisse, G. Watelle-Marion, J. Inorg. Nucl. Chem. 40 (1978) 819.
[14] D. Dollimore, G.R. Heal, J. Mason, Thermochim. Acta 24 (1978) 307.
[15] Y. Masuda, K. Nagagata, Thermochim. Acta 155 (1989) 255.
[16] Y. Masuda, K. Hirata, Y. Ito, Thermochim. Acta 203 (1992) 289.
[17] J.A. Lumpkin, D.D. Perlmutter, Thermochim. Acta 249 (1955) 335.
[18] B.V. L'vov, A.V. Novichikhin, A.O. Dyakov, Thermochim. Acta 315 (1998) 135.
[19] B.V. L'vov, Thermochim. Acta 315 (1998) 145.
[20] A.K. Kikoin, I.K. Kikoin, Molecular Physics, Nauka, Moscow, 1986 (in Russian).
[21] H.W. Quinn, R.W. Missen, G.B. Frost, Can J. Chem. 33 (1955) 286.